M&C 2017 - International Conference on Mathematics & Computational Methods Applied to Nuclear Science & Engineering, Jeju, Korea, April 16-20, 2017, on USB (2017)

Improvement of the 2D/1D Method in MPACT Using the Subplane Scheme[1]

Aaron M. Graham,* Benjamin S. Collins,† Thomas Downar*

*Department of Nuclear Engineering and Radiological Sciences, University of Michigan, Ann Arbor, MI
†Oak Ridge National Laboratory, P.O. Box 2008, Oak Ridge, TN
aarograh@umich.edu, collinsbs@ornl.gov, downar@umich.edu

Abstract - *Oak Ridge National Laboratory and the University of Michigan are jointly developing the MPACT code to be the primary neutron transport code for the Virtual Environment for Reactor Applications (VERA). To solve the transport equation, MPACT uses the 2D/1D method, which decomposes the problem into a stack of 2D planes that are then coupled with a 1D axial calculation. MPACT uses the method of characteristics (MOC) for the 2D transport calculations and 1D P_3 wrapped in a two-node nodal expansion method (NEM-P_3) solver for the 1D axial calculations, then accelerates the solution using the 3D coarse mesh finite difference (CMFD) method. Increasing the number of 2D MOC planes will increase the accuracy of the calculation, but will also increase the computational burden of the calculations and can result in slow convergence or instability. To prevent these problems while maintaining accuracy, the subplane scheme has been implemented in MPACT. This method subdivides the MOC planes into subplanes, refining the 1D NEM-P_3 and 3D CMFD calculations. This allows fewer MOC planes to be used while maintaining accuracy, improving the stability, and decreasing the required computational resources.*

To test the subplane scheme, three of the VERA Progression Problems were selected: Problem 3, a single assembly problem; Problem 4, a 3×3 assembly problem with control rods and pyrex burnable poisons; and Problem 5, a quarter-core problem. These three problems demonstrated that the subplane scheme can accurately produce intra-plane axial flux profiles that preserve the accuracy of the fine mesh solution. The eigenvalue differences are negligibly small, and differences in 3D power distributions are less than 0.1% for realistic axial meshes. Furthermore, the convergence behavior with the subplane scheme compares favorably with the conventional 2D/1D method, and the computational expense is decreased for all calculations owing to the reduction in expensive MOC calculations.

I. INTRODUCTION

The Consortium for Advanced Simulation of Light-Water Reactors [1] is currently developing an advanced code package called the Virtual Environment for Reactor Applications (VERA). VERA is intended to provide tools for high-fidelity modeling and simulation of light-water reactors beyond what has so far been possible with tools available to industry. VERA's tools include codes to perform neutronics, thermal-hydraulics, fuel performance, and other calculations, as shown in Figure 1. MPACT is the deterministic neutronics code in VERA that uses the 2D/1D method to provide 3D pin-resolved power distributions for the entire reactor [2, 3]. The work discussed in this paper focuses on improvements made to the 2D/1D implementation in MPACT using the subplane scheme.

The 2D/1D method [3, 4, 5, 6] takes advantage of the geometry in the reactor by noting that most of the heterogeneity occurs in the radial direction. Because of this feature, the problem is decomposed into a stack of 2D planes. In MPACT, each

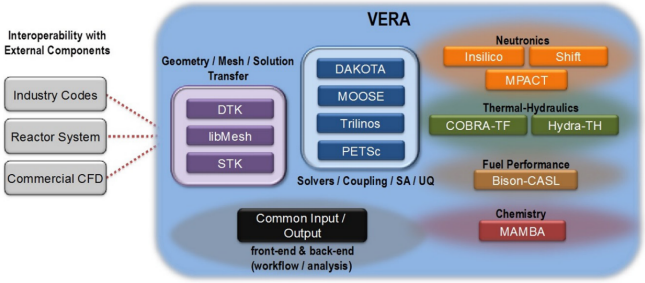

Fig. 1. VERA code package.

of these radial planes is solved using the 2D method of characteristics (MOC), which is capable of accurately resolving complicated geometries. These planes are then coupled axially using the 1D P_3 approximation wrapped in a two-node nodal expansion method (NEM-P_3) [7, 8] calculation on a coarse, pin-homogenized mesh. Additionally, this scheme uses the 3D coarse mesh finite difference (CMFD) method [9] to accelerate the convergence of the solution. This iteration scheme is capable of providing highly accurate 3D power distributions and is still much faster than doing a direct 3D transport calculation. However, the cost of direct whole-core transport calculations using the 2D/1D method significantly increased computational cost compared to current methods— with the majority of the computational burden coming from the 2D MOC calculations.

[1]This manuscript has been authored by UT-Battelle, LLC, under Contract No. DE-AC0500OR22725 with the U.S. Department of Energy. The United States Government retains and the publisher, by accepting the article for publication, acknowledges that the United States Government retains a nonexclusive, paid-up, irrevocable, worldwide license to publish or reproduce the published form of this manuscript, or allow others to do so, for the United States Government purposes. The Department of Energy will provide public access to these results of federally sponsored research in accordance with the DOE Public Access Plan (http://energy.gov/downloads/doe-public-access-plan).

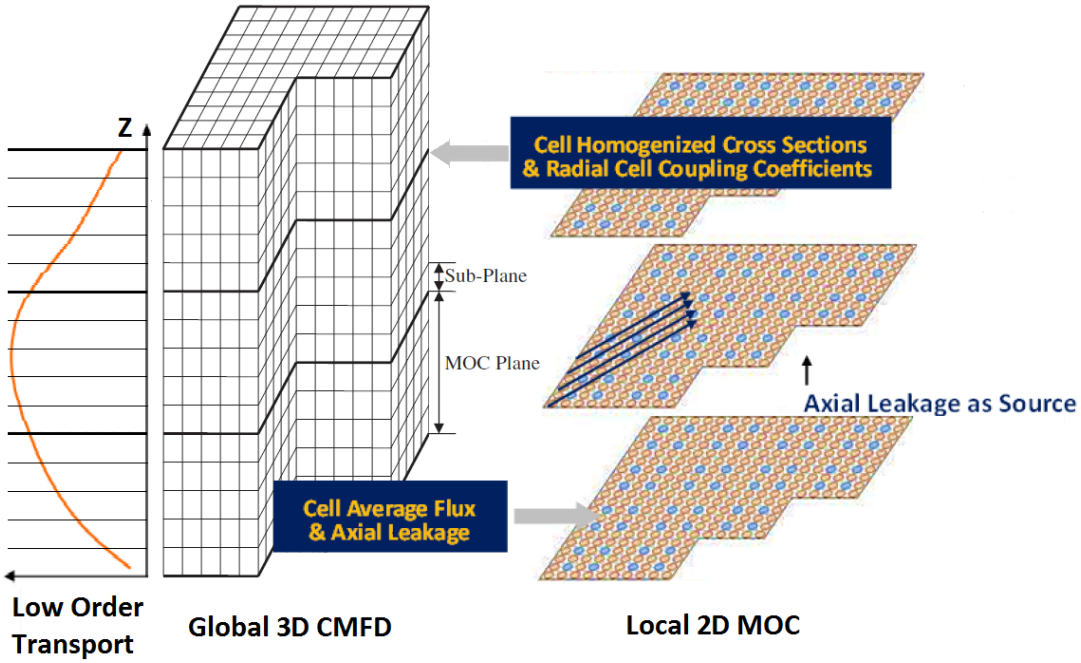

Fig. 2. The 2D/1D method with the subplane scheme used for the 3D CMFD and 1D axial calculations.

Because of this, a balance must be struck between minimizing the number of MOC planes to reduce runtime and maintaining a sufficiently accurate solution. This paper will discuss the subplane scheme, which is an alternative way of using the CMFD and 1D NEM-P_3 solvers to reduce the number of MOC planes without sacrificing solution accuracy.

II. THEORY

The subplane scheme, depicted in Figure 2 and described here, is a modification to the manner in which the 3D CMFD system and 1D axial solvers interact with the 2D MOC planes. To expound on the subplane scheme, first, the traditional CMFD method will be introduced and briefly explained. Then the modifications required for the implementation and use of the subplane scheme to be used will be discussed. Finally, the iteration scheme for the CMFD calculations and a full 2D/1D calculation in MPACT will be discussed.

1. CMFD Acceleration

CMFD is a coarse mesh acceleration method that can be used with a variety of transport methods [9]. To accelerate convergence, the MOC mesh used by the transport calculations is homogenized into a coarser mesh. The diffusion approximation is then applied to this coarse mesh. This produces a linear system for $N \times G$ unknowns, where N is the total number of CMFD cells and G is the number of energy groups used by the problem. Solving this system provides a global flux shape on the coarse mesh. This shape can be used to scale the fine mesh fluxes to accelerate convergence and to calculate an updated eigenvalue for the eigenvalue problem.

In MPACT, a single pin cell usually contains around 50 fine mesh regions for which the scalar flux is calculated using MOC. To prepare the coarse mesh, each of these pin cells is homogenized into a single coarse mesh cell with an axial height equal to the thickness of the MOC plane. This procedure is applied to every pin cell in each MOC plane as shown in Equation 1:

$$V_J = V_I = \sum_{i \in I} V_i \,, \tag{1a}$$

$$\phi^k_{g,J} = \phi^{k-1}_{g,I} = \frac{\sum_{i \in I} \phi^{k-1}_{g,i} V_i}{V_J} \,, \tag{1b}$$

$$\Sigma^k_{g,J} = \Sigma^{k-1}_{g,I} = \frac{\sum_{i \in I} \phi^{k-1}_{g,i} \Sigma^{k-1}_{g,i} V_i}{\sum_{i \in I} \phi^{k-1}_{g,i} V_i} \,, \tag{1c}$$

$$\chi^k_{g,J} = \chi^{k-1}_{g,I} = \frac{\sum_{i \in I} \chi^{k-1}_{g,i} \sum_{g' \in G} \phi^{k-1}_{g',i} \nu\Sigma^{k-1}_{f,g',i} V_i}{\sum_{i \in I} \sum_{g' \in G} \phi^{k-1}_{g',i} \nu\Sigma^{k-1}_{f,g'i} V_i} \,, \tag{1d}$$

where i is the fine mesh cell index, I is the set of fine mesh cells that make up the coarse mesh cell, J is the coarse mesh cell index, g indicates the energy group index, V is volume, k is the iteration index, ϕ is the scalar flux, Σ is a transport or scattering cross-section, $\nu\Sigma_f$ is the nu-fission cross-section, and χ is the energy distribution for the fission source. Using these definitions, the coarse mesh quantities preserve the volume-averaged scalar flux and reaction rates in each pin cell on the MOC mesh—which is necessary for consistency between the MOC and CMFD calculations.

For consistency, ensuring that the leakage on each face of the pin cell is consistent between the transport and diffusion solutions is a requirement. Because the CMFD system is using the diffusion approximation, the currents calculated at the coarse mesh cell interfaces will differ from those calculated

using MOC. To prevent this inconsistency, a current correction factor is calculated using the transport solution that enforces consistency between the CMFD and MOC currents. These correction factors are calculated for each of the six faces of the coarse mesh cell, as shown in Equation 2:

$$J_{g,J+\frac{1}{2}} = -D_{g,J+\frac{1}{2}}\left(\phi_{g,J+1} - \phi_{g,J}\right) + \hat{D}_{g,J+\frac{1}{2}}\left(\phi_{g,J+1} + \phi_{g,J}\right) , \tag{2a}$$

$$D_{g,J+\frac{1}{2}} = \frac{1}{3\left(\Delta_{j+1}\Sigma_{tr,g,J+1} + \Delta_j\Sigma_{tr,g,J}\right)} , \tag{2b}$$

$$\hat{D}_{g,J+\frac{1}{2}} = \frac{J_{g,I+\frac{1}{2}} + D_{g,J+\frac{1}{2}}\left(\phi_{g,J+1} - \phi_{g,J}\right)}{\phi_{g,J+1} + \phi_{g,J}} . \tag{2c}$$

As before, i refers to fine mesh cells, and J refers to coarse mesh cells. Indexes $I+\frac{1}{2}$ and $J+\frac{1}{2}$ refer to the same interface between two pin cells, with $I+\frac{1}{2}$ referring the quantities from the transport calculation and $J+\frac{1}{2}$ referring to the quantities from the diffusion calculations. Δ_J is half the width of pin cell J, and $\Sigma_{tr,g,J}$ is the group g transport cross-section for CMFD cell J. $D_{g,J+\frac{1}{2}}$ is the group g diffusion coefficient at interface $J+\frac{1}{2}$, and $\hat{D}_{g,J+\frac{1}{2}}$ is the group g coupling coefficient enforcing consistency between the diffusion and transport solutions at the same interface. In MPACT, the transport current $J_{g,I+\frac{1}{2}}$ comes from the 2D MOC calculations for the four radial interfaces and the 1D NEM-P_3 calculations for the two axial interfaces. These definitions ensure consistency between the CMFD and MOC solutions as well as between the CMFD and axial NEM-P_3 solutions.

After the CMFD calculation has finished, the MOC flux must be scaled using the CMFD results by simply calculating a scaling factor using the new and old CMFD fluxes, then applying this scaling factor to each of the MOC fluxes in the CMFD pin cell. This process accelerates the convergence of the transport solution by correcting the magnitude of the fine mesh fluxes while preserving the intra-pin shape calculated by MOC. This process is shown in Equation 3:

$$\phi^k_{g,i} = \frac{\phi^k_{g,J}}{\phi^{k-1}_{g,J}}\phi^{k-1}_{g,i} . \tag{3}$$

2. Subplane Scheme

The conventional 2D/1D approach requires a carefully selected axial mesh. A refined axial mesh can lead to instabilities in the 2D/1D iteration scheme [10] and increased computational cost due to more MOC calculations. However, coarsening the axial mesh too much can decrease the accuracy of the 2D/1D approach. To solve this problem, a group of researchers at the Korea Atomic Energy Research Institute developed the subplane scheme [11]. This scheme allows each pin cell in the coarse mesh to be divided axially into multiple cells. Thick MOC planes can then be used to minimize instability and computational burden while the CMFD and 1D NEM-P_3 calculations generate intra-plane flux profiles as if a finer axial mesh were being used.

To describe this scheme, some notation must be defined. Subscripts i and j will refer to fine mesh and coarse mesh cell indexes, respectively. I is then defined as the set of fine mesh cells making up a pin cell in the MOC mesh, and J is the set of coarse mesh cells used by CMFD and then axial NEM-P_3 that make up a full pin cell in the MOC mesh. Using this notation, cell-averaged volume and flux from the MOC mesh relates to the plane-averaged volume and flux from the CMFD mesh, as follows:

$$\sum_{i\in I} V_i = V_I = V_J = \sum_{j\in J} V_j , \tag{4a}$$

$$\frac{1}{V_I}\sum_{i\in I}\phi_{g,i}V_i = \phi_{g,I} = \phi_{g,J} = \frac{1}{V_J}\sum_{j\in J}\phi_{g,j}V_j . \tag{4b}$$

With this notation defined, the CMFD method using the subplane scheme can now be described. First, a subplane shaping factor s is calculated for each CMFD cell. This factor is used to provide an axial shape for the cross-sections since homogenization of the MOC mesh will not accomplish this on its own. To do this, the ratio of the CMFD cell flux to the previous iteration's plane-averaged CMFD flux is used to generate a shape function for each CMFD cell, as shown in equation 5:

$$s^k_{g,j} = \begin{cases} \frac{\phi^{k-1}_{g,j}}{\phi^{k-1}_{g,J}} & , \ k > 1 \\ 1 & , \ k = 1 \end{cases} . \tag{5}$$

With this factor defined, we can now define the homogenized flux, cross-sections, and χ for each CMFD cell using the most recent MOC and CMFD solutions. To account for the intra-plane axial profiles, the fine mesh flux ϕ_i is multiplied by the shaping factor s_j for each CMFD cell, giving the following modified equations:

$$\phi^k_{g,j} = \frac{\sum_{i\in I} s^k_{g,j}\phi^{k-1}_{g,i}V_i}{V_J} , \tag{6a}$$

$$\Sigma^k_{g,j} = \frac{\sum_{i\in I} s^k_{g,j}\phi^{k-1}_{g,i}\Sigma^{k-1}_{g,i}V_i}{\sum_{i\in I} s^k_{g,j}\phi^{k-1}_{g,i}V_i} , \tag{6b}$$

$$\chi^k_{g,j} = \frac{\sum_{i=1}^{I}\chi_{g,i}\sum_{g'\in G} s^k_{g',j}\phi^{k-1}_{g',i}\nu\Sigma^{k-1}_{f,g',i}V_i}{\sum_{i=1}^{I}\sum_{g'\in G} s^k_{g',j}\phi^{k-1}_{g',i}\nu\Sigma^{k-1}_{f,g',i}V_i} . \tag{6c}$$

The homogenized cross-sections in Equation 6b has the axial shaping factor $s_{g,j}$ in both summations. Because the shaping factor is constant radially, it cancels out and gives an expression equivalent to Equations 1c:

$$\Sigma^k_{g,j} = \frac{\sum_{i\in I}\phi^{k-1}_{g,i}\Sigma^{k-1}_{g,i}V_i}{\sum_{i\in I}\phi^{k-1}_{g,i}V_i} = \Sigma^k_{g,J} . \tag{7}$$

With this simplification, the cross-sections are axially constant, and χ has an axial distribution within each MOC plane. This result is expected and physically consistent. A fundamental assumption of the 2D/1D method is that the materials are constant in each plane, so the cross-sections should remain axially constant within the plane, even with the application

of the subplane scheme. However, the axial mesh refinement introduced by the subplane scheme should also have the effect of refining the fission source distribution. This is accomplished by allowing χ to have an intra-plane axial shape.

The current coupling coefficients described in Equation 2 also require some modification. With the subplane scheme, each pin cell has multiple interfaces in the axial direction, and each radial interface has one sub-interface for each subplane. Because the 1D NEM-P_3 calculations use the same homogenized mesh as the subplane CMFD calculations, the radial and axial coupling coefficients must be handled differently. In the radial direction, the transport currents have been calculated along the entire interface. Thus, the other quantities must also be calculated for full height of the MOC plane. To accomplish this, the following equations for the radial diffusion currents are defined:

$$J_{rad,g,j+\frac{1}{2}} = -D_{rad,g,J+\frac{1}{2}}\left(\phi_{g,j+1}-\phi_{g,j}\right) + \hat{D}_{rad,g,J+\frac{1}{2}}\left(\phi_{g,j+1}-\phi_{g,j}\right), \quad (8a)$$

$$D_{rad,g,J+\frac{1}{2}} = \frac{1}{3\left(\Delta_{j+1}\Sigma_{tr,g,j+1}+\Delta_j\Sigma_{tr,g,j}\right)}, \quad (8b)$$

$$\hat{D}_{rad,g,J+\frac{1}{2}} = \frac{J_{rad,g,I+\frac{1}{2}} + D_{rad,g,J+\frac{1}{2}}\left(\phi_{g,J+1}-\phi_{g,J}\right)}{\phi_{g,J+1}+\phi_{g,J}}. \quad (8c)$$

Using these definitions, the coupling coefficients D and $\hat{D}$ are the same for all sub-interfaces on a given radial interface. However, the subplane fluxes are used in the calculation of the radial currents, allowing the currents to maintain an intra-plane axial shape.

For the axial interfaces, subplane quantities are used everywhere instead of the plane-averaged quantities, giving Equation 9:

$$J_{ax,g,j+\frac{1}{2}} = -D_{ax,g,j+\frac{1}{2}}\left(\phi_{g,j+1}-\phi_{g,j}\right) + \hat{D}_{ax,g,j+\frac{1}{2}}\left(\phi_{g,j+1}-\phi_{g,j}\right), \quad (9a)$$

$$D_{ax,g,j+\frac{1}{2}} = \frac{1}{3\left(\Delta_{j+1}\Sigma_{tr,g,j+1}+\Delta_j\Sigma_{tr,g,j}\right)}, \quad (9b)$$

$$\hat{D}_{ax,g,j+\frac{1}{2}} = \frac{J_{ax,g,i+\frac{1}{2}} + D_{ax,g,j+\frac{1}{2}}\left(\phi_{g,j+1}-\phi_{g,j}\right)}{\phi_{g,j+1}+\phi_{g,j}}. \quad (9c)$$

Using these expressions, each axial interface in a pin cell has a unique set of D and $\hat{D}$, unlike the radial interfaces, which use a single value for D and $\hat{D}$ for all sub-interfaces in each direction. However, this is required to maintain consistency between the CMFD and 1D NEM-P_3 systems.

Equation 3 can be used, without modification, to project the CMFD flux back to the MOC fine mesh. This equation requires the CMFD flux to be averaged over the entire plane. For traditional CMFD, this is immediately available at the end of the calculation. When applying the subplane scheme, the subplane cells must be volume-averaged in each MOC plane to obtain $\phi^k_{g,J}$ and $\phi^{k-1}_{g,J}$. This averaging is accomplished by applying Equation 4b to the solutions of the current and previous iterations.

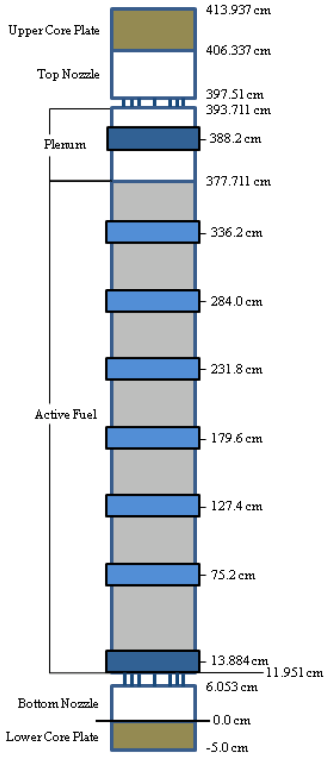

Fig. 3. Axial view of Westinghouse 17×17 fuel assembly in Watts Bar Unit 1.

III. RESULTS AND ANALYSIS

When testing the subplane scheme, there are two primary concerns. First, it is important to determine if the subplane scheme is preserving the accuracy of an axially refined conventional 2D/1D calculation. It must be shown that the intra-plane flux profiles calculated by CMFD and 1D NEM-P_3 compare well with the profiles obtained by simply adding more MOC planes. 3D pin power distributions and k_{eff} are used to show this comparison. Second, the convergence and runtime behavior must also be analyzed. Increasing the number of iterations required to converge can be prohibitive when introducing complications such as coupling with other codes for thermal-hydraulic or fuel performance feedback. Furthermore, the subplane scheme introduces some parallel imbalance in the CMFD and axial NEM-P_3 systems that could increase the computational expense, even if the calculations converge in the same number of iterations. The efficiency of the subplane scheme is analyzed by counting the number of iterations and the runtime (core-hours) required to reach convergence.

Three models were taken from the VERA Progression Problems [12], based on Watts Bar Unit 1, and used to test the subplane scheme. All problems use Westinghouse 17×17 fuel assemblies, shown in Figure 3, with active fuel heights of 365.76 cm. Each assembly has six spacer grids in the active fuel region, with a height of 3.810 cm. Using conventional 2D/1D, these problems would normally be simulated using a total of 58 MOC planes, with 49 planes in the active fuel region. Each spacer grid is one plane, and the spans between grids are divided into 6 planes, each being about 8 cm thick. All three

TABLE I. Comparison of subplane scheme to traditional 2D/1D for VERA Progression Problem 3a.

Planes	Number of Cores		k-eff Difference	Pin Power Difference		Outer Iterations		Runtime (Core-hours)		Speedup
	Conventional	Subplane	(pcm)	RMS	Max	Conventional	Subplane	Conventional	Subplane	
44	44	30	0.0	0.015%	0.048%	11	11	0.58	0.45	1.29
58	58	30	0.0	0.029%	0.095%	9	9	0.75	0.44	1.71
88	44	30	0.1	0.024%	0.090%	9	9	0.95	0.57	1.67
106	53	30	−0.2	0.046%	0.139%	9	9	1.14	0.65	1.76
147	49	30	0.0	0.072%	0.172%	17	9	2.40	0.97	2.46

problems take advantage of symmetry, allowing MPACT to model only the southeastern quadrant of the problem.

These models were meshed to enable a comparison between an axially refined 2D/1D mesh without the subplane scheme and an axially coarse 2D/1D mesh with the subplane scheme. For each problem, all subplane calculations used the same number of MOC planes with an increasingly refined subplane mesh. This was accomplished by sub-dividing all MOC planes into subplanes until they were less than a user-specified maximum thickness, ranging from 3.2–19 cm. For each of these subplane cases, a reference was set up that had one MOC plane for each subplane in the test case. This configuration resulted in the mesh for the CMFD and NEM-P_3 calculations being identical between the two models while the number of MOC planes in the reference case was higher. An example of this meshing scheme is shown in Figure 4.

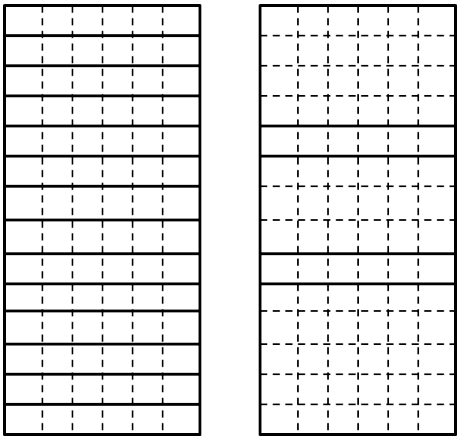

Fig. 4. Depiction of conventional (left) and subplane (right) 2D/1D axial meshes. Solid lines indicate MOC plane boundaries, while dashed lines indicate CMFD cell boundaries.

1. VERA Problem 3a

The first problem is Progression Problem 3a, which consists of a single assembly with 2.6% enrichment. No control rods or burnable poisons are present in this problem. The model has also been modified to exclude the spacer grids. The spacer grids are modeled for the full axial height of an MOC plane, and without their removal this would cause—for the most refined meshes tested in this paper— differences between the reference cases and subplane cases that are not caused by using the subplane scheme. Removal of the spacer grids provides a more consistent comparison between conventional and subplane 2D/1D, even though both methods can accurately capture spacer grid effects.

Table I shows the results for the Problem 3a calculations. Each subplane case was executed using 30 MOC plane on a development cluster running 16 8-core AMD Opteron^{TM} Processor 6376 CPUs clocked at 2.3 GHz. The first column shows the total number of subplanes in the test cases and the number of MOC planes used for the conventional 2D/1D reference cases. In all cases, the k_{eff} differences are negligibly small, being on the order of the k_{eff} convergence criterion of 0.1 pcm. The power distribution errors show a generally increasing trend as the mesh is refined. As more MOC planes are added to the reference cases, the differences in the transport solution—at each axial level that CMFD is unable to capture—are expected to grow. However, even with 147 planes, the RMS difference in the power distribution is only 0.07%, and the maximum difference is only 0.172%. For the 58-plane cases, which are closest to the mesh normally used for Problem 3a, the maximum difference is less than 0.1%—a negligibly small difference.

The convergence of the subplane cases is much more consistent than the conventional 2D/1D case. The 44-subplane case, which had a maximum subplane thickness of 14.3695 cm, required 11 iterations to converge. Because all other subplane cases had thinner CMFD cells and the same MOC plane thicknesses, each of them took 9 iterations. The conventional cases showed more fluctuations. The 88-plane case converged in just 7 iterations, but the more refined meshes began requiring more iterations because of the thinner MOC planes, with the 147-plane case requiring as many as 17 iterations. This occurs because the thinner MOC planes increase the under-relaxation required for 2D/1D, which slows the convergence.

The runtime in terms of core-hours is consistently less for the subplane cases than for the conventional 2D/1D cases. This is caused primarily by the subplane cases having only one MOC plane per core, no matter how refined the axial mesh was. The conventional cases used more cores and had as many as three MOC planes per core, which significantly increased the computational expense. Furthermore, the increased number of cores used in the parallel decomposition also reduces the parallel efficiency of the calculation. Since only planar decomposition was being used, this effect would be observed primarily in the CMFD method, with some effect on the 1D NEM-P_3 and little effect on the 2D MOC. While these effects are greater for the conventional 2D/1D cases, the subplane

TABLE II. Comparison of subplane scheme to traditional 2D/1D for VERA Progression Problem 4.

Planes	Number of Cores		k-eff Difference	Pin Power Difference		Outer Iterations		Runtime (core-hours)		Speedup
	Conventional	Subplane	(pcm)	RMS	Max	Conventional	Subplane	Conventional	Subplane	
44	44	30	0.0	0.020%	0.127%	12	13	6.26	4.98	1.26
58	58	30	0.0	0.006%	0.027%	12	12	10.67	5.50	1.94
88	44	30	0.0	0.006%	0.039%	12	12	11.88	6.28	1.89
106	53	30	−0.7	0.086%	0.289%	13	12	19.17	7.42	2.58
147	49	30	−0.6	0.088%	0.282%	18	12	30.04	9.89	3.04

cases have a unique parallel imbalance. Because the decomposition is done according to the MOC planes, dividing the MOC planes into subplanes causes the CMFD system to have a parallel imbalance for the subplane cases—an imbalance that cannot exist for the conventional 2D/1D cases. If this imbalance were eliminated, the speedup from subplane would increase further.

2. VERA Problem 4

The second problem is Progression Problem 4, a 3×3 assembly problem. This problem has a combination of 2.1% and 2.6% enriched assemblies. The center assembly has a control rod, and some of the other assemblies have discrete pyrex burnable poisons. The control rod and burnable poison positions were adjusted slightly to align with the top or bottom of spacer grid planes. This positioning prevents potential discrepancies caused by homogenizing materials while using coarse axial meshes. Additionally, the spacer grid material was removed from the model, as with Problem 3. The assembly layout is shown in Figure 5.

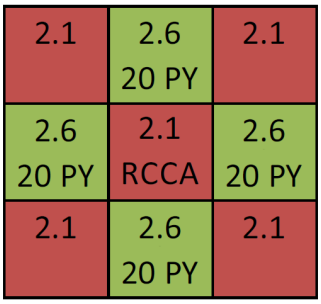

Fig. 5. VERA Problem 4 assembly layout.

The Problem 4 results are shown in Table II. The k_{eff} differences are once again negligibly small at less than 1 pcm for all subplane cases. For the 3 coarsest meshes, the power differences are comparable to the Problem 3 results. The two finest meshes show maximum differences larger than for Problem 3, close to 0.3%. However, this is still a small difference, and it occurs near the bottom of the problem at the interface between the pyrex poison and the end plug, where the power is low.

The Problem 4 calculations used the same planar decomposition scheme used for Problem 3 and were conducted on the same development machine. The convergence behavior is similar for the conventional and subplane cases, except for the more refined conventional case. The runtime improvement of the subplane cases is more significant for Problem 4 that for Problem 3. This occurs because each parallel domain in Problem 3 consists of a quarter assembly; whereas for Problem 4, each domain consists of 2.25 total assemblies. Thus, the reduction in MOC planes becomes more significant for Problem 4. The speedup is around 2× for the 58-plane case, and exceeds 3× for the most refined 147-plane case.

3. VERA Problem 5

The third problem is Progression Problem 5. This problem is the full Watts Bar Unit 1 core at beginning of life, including radial reflector regions. Enrichments for this problem range from 2.1% to 3.1%. All control banks are fully withdrawn except for bank D, which is inserted about $\frac{1}{3}$ of the way into the active fuel region. Some assemblies also have burnable pyrex rods. The radial layout of Problem 5 is shown in Figure 6. The same adjustments as were made in the previous two models were also made here—to spacer grids, control rods, and burnable poisons.

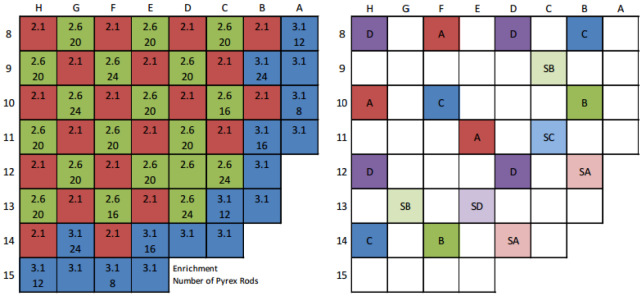

Fig. 6. VERA Problem 5 assembly layout.

Problem 5 was run on Oak Ridge National Laboratory's Titan [13] using 16 CPU cores per MOC plane. The results are shown in Table III. Overall, the k_{eff} and power distribution differences for each case are similar to those of Problem 4. The subplane cases still showed speedup compared with the conventional cases, but not as much of a speedup as seen in Problems 3 and 4. This performance shortfall is caused primarily by the increase in the CMFD system's size, which results in an increase in the parallel imbalance for the subplane cases. Furthermore, this CMFD imbalance also required more nodes to be used for the subplane calculations due to the increase in memory requirements.

It should be noted that the 106-plane conventional 2D/1D

TABLE III. Comparison of subplane scheme to traditional 2D/1D for VERA Progression Problem 5.

Planes	Number of Cores		k-eff Difference	Pin Power Difference		Outer Iterations		Runtime (core-hours)		Speedup
	Conventional	Subplane	(pcm)	RMS	Max	Conventional	Subplane	Conventional	Subplane	
44	704	480	0.0	0.006%	0.035%	12	12	192	174	1.11
58	928	480	−0.1	0.008%	0.065%	13	12	264	213	1.24
88	1408	480	−0.1	0.008%	0.120%	13	12	416	294	1.41
106	1696	480	−0.3	0.058%	0.229%	13	13	520	397	1.31
147	2352	480	−0.3	0.057%	0.220%	18	12	962	477	2.02

case and both 147-plane cases experienced convergence issues that required some small adjustments to the axial calculations. These adjustments did not affect the runtime or accuracy, but did indicate that the thick MOC planes used by the subplane scheme served to maintain stability at finer meshes than the conventional 2D/1D approach. The combination of thicker MOC planes and thinner CMFD planes can improve stability in some cases.

IV. CONCLUSIONS AND FUTURE WORK

The subplane scheme was successfully implemented in the MPACT 2D/1D code. VERA Progression Problems 3a, 4, and 5 were simulated using a variety of different conventional and subplane meshes to analyze the performance of the subplane scheme. All three problems showed that the subplane scheme sufficiently preserves the intra-plane flux shape from a more refined 2D/1D calculation. Furthermore, these runs showed that using the subplane scheme decreased the computational expense for all three problems.

However, several improvements can still be made to this implementation. First, the subplane scheme naturally introduces an imbalance in the CMFD system for parallel calculations. This imbalance decreases the parallel efficiency and increases the memory requirements for each core, though the total memory usage is less than that of a more refined conventional 2D/1D calculation. This could be improved by decomposing the CMFD system separately from the MOC calculation to improve the parallel efficiency and to more evenly distribute the memory burden.

A second improvement to the subplane scheme involves stability. For some of the more finely meshed subplane cases for Problems 4 and 5, the iteration scheme became unstable. To mitigate this instability required switching from the default one-node NEM-P_3 axial solvers to a hybrid solver that produces the same solution as the one-node solver but displays better stability for certain problems. While all the calculations for this paper were successfully completed using one of these two solvers, an axial solver that remains stable with thin subplanes would make the subplane scheme more reliable and user friendly. These two axial solvers are discussed in further detail in [14].

Finally, the 2D/1D method fundamentally assumes that materials are axially constant within each MOC plane. When this is not true, the materials must be axially homogenized to perform the 2D MOC calculations. The most common example of this is control rod cusping [7], which introduces large errors caused by the volume homogenization of strongly absorbing control rod materials in the 2D MOC plane. Therefore, to improve the practical usefulness of the subplane scheme, an accurate and efficient control rod decusping technique must be used to correct the cusping errors. A variety of solutions have been developed to address this problem [15, 16, 17], including one which has been developed in MPACT specifically for the subplane 2D/1D framework [18].

V. ACKNOWLEDGMENTS

This material is based upon work supported under an Integrated University Program Graduate Fellowship.

This research was supported by the Consortium for Advanced Simulation of Light Water Reactors (www.casl.gov), an Energy Innovation Hub (http://www.energy.gov/hubs) for Modeling and Simulation of Nuclear Reactors under U.S. Department of Energy Contract No. DE-AC05-00OR22725.

This research also made use of resources of the Oak Ridge Leadership Computing Facility at the Oak Ridge National Laboratory, which is supported by the Office of Science of the U.S. Department of Energy under Contract No. DE-AC05-00OR22725.

REFERENCES

1. "Consortium for Advanced Simulation of Light Water Reactors (CASL)," Available online. URL www.casl.gov.
2. MPACT TEAM, "MPACT Theory Manual," Tech. rep., Oak Ridge National Laboratory and the University of Michigan (February 2015).
3. B. S. COLLINS, S. STIMPSON, B. W. KELLEY, M. T. H. YOUNG, B. KOCHUNAS, A. GRAHAM, E. W. LARSEN, T. DOWNAR, and A. GODFREY, "Stability and Accuracy of 3D Neutron Transport Simulations Using the 2D/1D Method in MPACT," *Journal of Computational Physics*, **326**, 612–628 (August 2016).
4. J. Y. CHO and H. G. JOO, "Solution of the C5G7MOX Benchmark Three-Dimensional Extension Problems by the DeCART Direct Whole Core Calculation Code," *Prog. Nucl. Energy*, **48**, 456–466 (2006).
5. H. G. JOO, J. Y. CHO, K. S. KIM, C. C. LEE, and S. Q. ZEE, "Methods and Performance of a Three-Dimensional Whole-Core Transport Code DeCART," in "PHYSOR 2004 – The Physics of Fuel Cycles and Advanced Nuclear Systems: Global Developments," Chicago, Illinois (April 25-29 2004).

6. Y. S. JUNG, H. G. JOO, ET AL., "Practical Numerical Reactor Employing Direct Whole Core Neutron Transport and Subchannel Thermal/Hydraulic Solvers," *Ann. Nucl. Energy*, **62**, 357–374 (2013).
7. H. FINNEMANN, F. BENNEWITZ, and M. WAGNER, "Interface current techniques for multidimensional reactor calculations," *Atomkernenergie*, **30**, *2*, 123–128 (1977).
8. R. G. MCCLARREN, "Theoretical Aspects of the Simplified Pn Equations," *Transport Theory and Statistical Physics*, **39**, *2-4*, 73–109 (2011).
9. K. SMITH, "Nodal Method Storage Reduction by Nonlinear Iteration," *Trans. Am. Nucl. Soc.*, **44**, 265 (1983).
10. B. W. KELLEY, *An Investigation of 2D/1D Approximation to the 3D Boltzmann Transport Equation*, Ph.D. thesis, University of Michigan (2015).
11. J. Y. CHO, K. S. KIM, C. C. LEE, S. Q. ZEE, and H. G. JOO, "Axial SP_N and Radial MOC Coupled Whole Core Transport Calculation," *Journal of Nuclear Science and Technology*, **44**, *9*, 1156–1171 (2007).
12. A. T. GODFREY, "VERA Core Physics Benchmark Progression Problem Specifications," Tech. rep., Oak Ridge National Laboratory (August 2014).
13. "Titan Cray XK7," Available online. URL https://www.olcf.ornl.gov/computing-resources/titan-cray-xk7/.
14. S. G. STIMPSON, B. S. COLLINS, A. ZHU, and Y. XU, "A Hybrid Nodal P_3/SP_3 Axial Transport Solver for the MPACT 2D/1D Scheme," in "PHYSOR 2016: Unifying Theory and Experiments in the 21st Century," Sun Valley, ID (May 1-5 2016).
15. H.-S. JOO, *Resolution of the control rod cusping problem for nodal methods*, Ph.D. thesis, Massachusetts Institute of Technology (1984).
16. J. C. GEHIN, "A quasi-static polynomial nodal method for nuclear reactor analysis," Tech. rep., Oak Ridge Inst. for Science and Education, TN (United States); Massachusetts Inst. of Tech., Cambridge, MA (United States) (1992).
17. Y. S. JUNG and H. G. JOO, "Control Rod Decusping Treatment Based on Local 3-D CMFD Calculation for Direct Whole Core Transport Solvers," in "Proceedings of the International Congress on Advances in Nuclear Power Plants (ICAPP)," (April 6–9 2014).
18. A. M. GRAHAM, B. S. COLLINS, and T. DOWNAR, "Rod Decusping Techniques for the 2D/1D Method," in "Proceedings of the International Conference on Mathematics and Computation (M&C 2017)," Jeju, Korea (April 2017).